© 3rd IAHR Europe Congress, Book of Proceedings, 2014, Porto - Portugal. ISBN 978-989-96479-2-3

EXPERIMENTAL CHARACTERIZATION OF DRAG ON ARRAYS OF ROUGH CYLINDERS

RICARDO, A.M.[1,2], MARTINHO, M.[3], SANCHES, P.[1],
FRANCA, M.J.[2] & FERREIRA, R.M.L.[1]

[1] *CEHIDRO Instituto Superior Técnico, Universidade de Lisboa, Lisboa, Portugal*

[2] *Laboratory of Hydraulic Constructions – École Polytechnique Fédéral de Lausanne, Switzerland*

[3] *Faculdade de Ciências e Tecnologia, Universidade Nova de Lisboa, Lisboa, Portugal*

ana.ricardo@ist.utl.pt; margalfmartinho@gmail.com; pedro.miguel.sanches@ist.utl.pt; mario.franca@epfl.ch; ruif@civil.ist.utl.pt

Abstract

Emergent vegetation, covering floodplains and wetlands, has an important role in fluvial ecosystems being able to control the fluxes of sediment, nutrients and contaminants. Proper understanding of flow resistance processes is crucial on the development of reliable tools for designing non-erodible channels.

The main objective of this study is the quantification of the forces, per unit bed area, acting on the stems and the respective coefficient. Particular goals include a characterization and quantification of the flow within vegetated areas susceptible to be simulated by dense arrays of vertical emergent stems and a discussion of the dependence of the drag coefficient on parameters that characterize this kind of flows.

To achieve the goals, experimental tests simulating rigid and emergent vegetation condition with varying and constant density of stems were performed. The data acquisition consisted mainly in 2D instantaneous velocities maps measured with a Particle Image Velocimetry system (PIV) and the data treatment was performed with the Double-Averaging methodology (DAM).

The flow characterization shows an important contribution of form-induced stresses, namely longitudinal and shear stresses which are of the order of magnitude of Reynolds stresses. Hence, in general, these stresses should not be neglected within the balance for the flow resistance. The results show that the drag force seems uncorrelated with the density of stems but impacted by the longitudinal variation of this. For the range of investigated Re_p and m, C_D seems uncorrelated with Re_p. C_D is larger for lower relative flow depths, revealing the influence of the channel.

Keywords: Rigid vegetation, Patchiness, PIV, Double-Averaging Methodology, Drag coefficient

1. Introduction

Emergent vegetation, covering floodplains and wetlands, has an important role in fluvial ecosystems, being able to control fluxes of sediment, nutrients and contaminants (Tanino and Nepf, 2008) and it provides a large range of ecosystem services (Aberle and Järvelä, 2013), allied to economical and safety functions as navigation and flood protection.

The characterization of drag forces on vegetation elements is one of the most important fields of research, with important applications in civil engineering, namely in the estimation of hydraulic resistance for design of fluvial channels or flood forecasting (Kadlec, 1990). Most of the existing design criteria and simulation models employ resistance formulas such as Manning's, necessarily calibrated *ad hoc*. Moving toward physically based design criteria, the Double-Averaging Methodology (DAM) allowed progress in the characterization of the 3D flow over irregular boundaries and over canopies (Finnigan, 2000; Nikora et al., 2007).

DAM is a particular form of upscaling in spatial and temporal sense. The conservation equations of turbulent flows are expressed for time-averaged quantities which, in case of unsteady flow, are defined in a time-window smaller than the fundamental unsteady flow time-scale, and for space-averaged quantities, defined in space windows larger than the characteristic wavelength of the boundary irregularities (Franca and Czernuszenko, 2006). DAM introduces a spatial decomposition which considers time-averaged flow variables divided into a spatial fluctuation component and a double-averaged value. Introducing the spatial decomposition into the well-known RANS, applying the space-averaged operator and following some theorems and mathematical rules, one obtains the Double-Averaged Navier-Stokes equations, DANS (Finnigan, 2000; Nikora et al., 2007). For incompressible and steady flows, DANS are given by

$$\begin{aligned}\langle \overline{u}_i \rangle \frac{\partial \langle \overline{u}_j \rangle}{\partial x_i} = -g_j - \frac{1}{\psi\rho}\frac{\partial \psi \langle \overline{p} \rangle}{\partial x_j} - \frac{1}{\psi}\frac{\partial \psi \langle \overline{u_i' u_j'} \rangle}{\partial x_i} - \frac{1}{\psi}\frac{\partial \psi \langle \tilde{u}_i \tilde{u}_j \rangle}{\partial x_i} + \frac{1}{\psi}\frac{\partial}{\partial x_i}\left(\psi \left\langle \nu \frac{\partial \overline{u}_j}{\partial x_i} \right\rangle\right) \\ + \frac{1}{\rho \forall_f^{(s)}} \int_{S_{int}^{(s)}} \overline{p} n_j \partial S - \frac{1}{\forall_f^{(s)}} \int_{S_{int}^{(s)}} \nu \frac{\partial \overline{u}_j}{\partial x_i} n_i \partial S + \frac{1}{\rho \forall_f^{(b)}} \int_{S_{int}^{(b)}} \overline{p} n_j \partial S - \frac{1}{\forall_f^{(b)}} \int_{S_{int}^{(b)}} \nu \frac{\partial \overline{u}_j}{\partial x_i} n_i \partial S\end{aligned} \quad [1]$$

where $i, j = x, y, z$ are the streamwise, spanwise and vertical directions, respectively, of the Cartesian referential, $\overline{u}_i$ and $\bar{p}$ are the i^{th} time-averaged velocity component and the and time-averaged pressure field, respectively, $\langle \overline{u}_i \rangle$ and $\langle \bar{p} \rangle$ are the mean (space- and time-averaged) velocities pressure, respectively, $\tilde{u}_i = \overline{u}_i - \langle \overline{u}_i \rangle$ stands for the spatial velocity fluctuations, ρ and ν are the fluid density and kinematic viscosity, respectively, and $\forall_f^{(k)}$and $S_{int}^{(k)}$ stand, respectively, for the volume of fluid and for the area of the fluid-solid interface of the control volume k. The volumetric fluid fraction defined as $\psi = 1 - \phi^{(s)} - \phi^{(b)}$ being $\phi^{(k)}$ the volumetric solid fraction in control volume k. $k = s$ identifies the control volume bounded by the mean bed elevation and the free surface and $k = b$ identifies the control volume bounded by a horizontal plane that contains the crests of the rough bed and by the mean bed elevation.

The stress and drag terms in Eq. [1] are: $-\rho\psi\langle \overline{u'_i u'_j} \rangle$ the Reynolds stress tensor; $-\rho\psi\langle \tilde{u}_i \tilde{u}_j \rangle$ the form-induced stress tensor; $\psi \langle \nu \frac{\partial \overline{u}_j}{\partial x_i} \rangle$ the viscous stress tensor; $\frac{1}{\rho \forall_f^{(s)}} \int_{S_{int}^{(s)}} \bar{p} n_j \mathrm{d}S$ the form (pressure) drag on the stems; $\frac{1}{\forall_f^{(s)}} \int_{S_{int}^{(s)}} \nu \frac{\partial \overline{u}_j}{\partial x_i} n_i \mathrm{d}S$ the viscous (skin) drag on the stems; $\frac{1}{\rho \forall_f^{(b)}} \int_{S_{int}^{(b)}} \bar{p} n_j \mathrm{d}S$ the form drag on the bed and $\frac{1}{\forall_f^{(b)}} \int_{S_{int}^{(b)}} \nu \frac{\partial \overline{u}_j}{\partial x_i} n_i \mathrm{d}S$ the viscous drag on the bed.

DAM will be applied in this work as a mean to obtain a physically based formulation to compute the drag force in flows within vegetation covered boundaries, susceptible of being simulated by arrays of rigid cylinders. Since natural systems are not homogeneous, the flow within the stem array is influenced by several space scales, determined by the number-density of stems and its spatial modulation.

The present work features the study of flows with and without spatial variability of the areal number-density of stems along the streamwise direction. The main objective is the quantification of the forces, per unit bed area, acting on the stems and the respective drag coefficient. Particular goals include a characterization and quantification of the flow within dense arrays of vertical emergent stems and a discussion of the dependence of the drag coefficient on parameters that characterize this kind of flows.

To achieve the proposed goals, two experimental tests were carried out. One of the tests featured a periodic distribution of stem areal number-densities with minimum and maximum values of 400 and 1600 stems/m^2. On the second test the same number of stems was distributed uniformly on the same area as the previous test, creating an array with stem areal number-density m=980 stems/m^2. The data acquisition consisted mainly in 2D instantaneous velocities maps measured with a Particle Image Velocimetry system (PIV).

This work is organized in four main sections. After the introduction, the experimental setup is described. Then, the results are presented and discussed and finally the paper is closed with the main conclusions.

2. Experimental tests

The experimental work was carried out in a 12.5 m long and 40.8 cm wide recirculating tilting flume of the Laboratory of Hydraulics and Environment of Instituto Superior Técnico. The flume has glass side walls, enabling flow visualization and laser illumination. A general representation of the flume is shown in Figure 1. The flume bottom was covered with a thin horizontal layer of gravel and sand and arrays of rigid, vertical and cylindrical stems were randomly placed along of a 3.5 m long reach simulating emergent vegetation conditions. The diameter of the cylindrical elements is 1.1 cm. Downstream the reach covered with vegetation, a coarse gravel weir controlled the flow, which was subcritical both downstream and upstream of the vegetated reach.

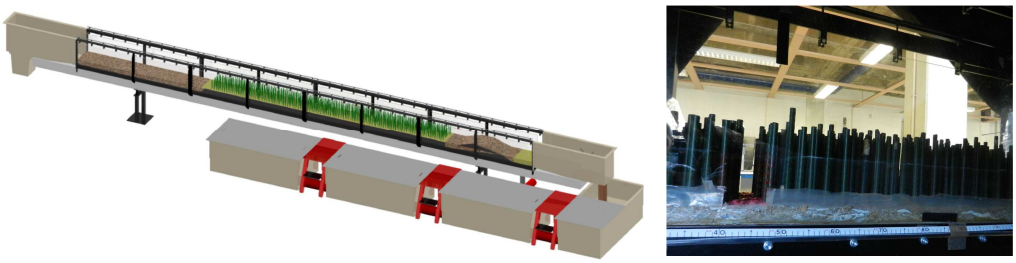

Figure 1. Schematic view of the recirculating tilting flume (left) and picture of the flume during the experiments (right).

Two experimental tests were performed: test A and test B, with spatially varying and constant stem areal number-density, respectively. For test A, the stems were placed in order to create a pattern with varying stem areal number-density with wavelength of 0.5 m (Figure 2 - top). Each wavelength comprises a 15 cm long patch with m =1600 stems/m^2 (dense patch, herein, $p_{0\text{-}1}$ and $p_{4\text{-}5}$); a 15 cm long patch with m=400 stems/m^2 (sparse patch, herein, $p_{2\text{-}3}$ and $p_{6\text{-}7}$); 10 cm long transitions patches with 980 stems/m^2 in average, divided into two 5 cm-long reaches with 1200 stems/m^2 and 800 stems/m^2 ($p_{1\text{-}2}$ and $p_{2\text{-}3}$ with decreasing m and $p_{3\text{-}4}$ and $p_{7\text{-}8}$ with increasing m).

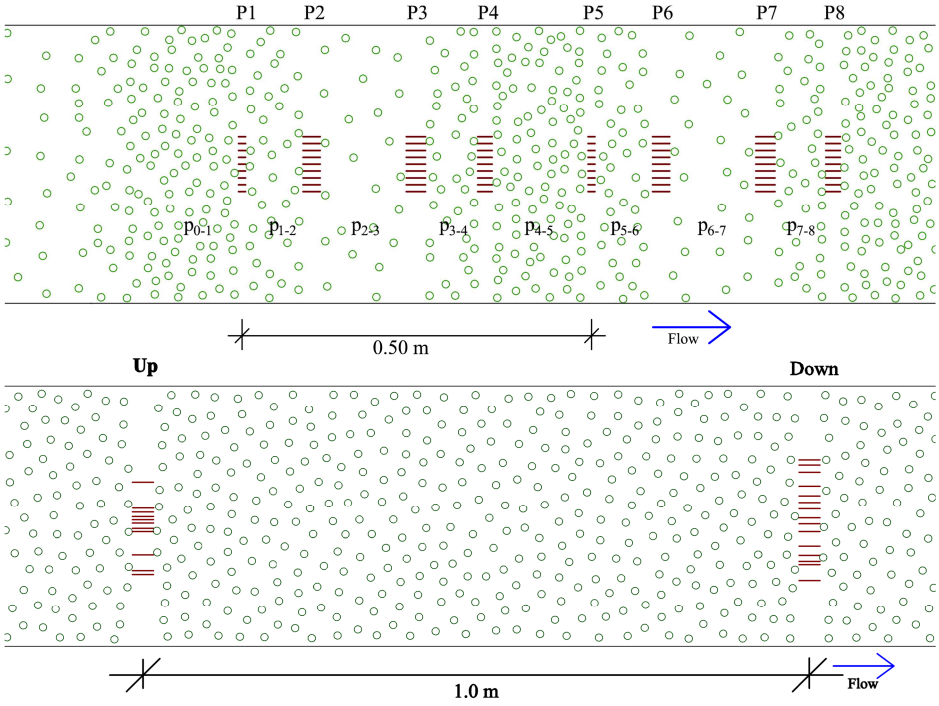

Figure 2. Plan view of test A (top) and B (bottom). The solid lines aligned with flow direction indicate the location of the vertical planes measured with PIV.

Test B was populated with the same number of stems of test A, distributed uniformly along the 3.5 m long reach, with random distribution, resulting in m=980 stems/m² (Figure 2 - bottom).

To enable velocity measurements, narrow regions without stems in the spanwise direction, herein called "measuring gaps", were enforced, whose width is equal to the mean inter-stem distance of the upstream reach. In test A data acquisition was carried out at eight measuring gaps, distributed along two wavelengths, P1 to P4 (first wavelength) and P5 to P8 (second wavelength), while in test B two measuring gaps 1.0 m apart were considered (Up and Down), as shown in Figure 2.

Measurements consisted in acquisition of 2D (streamwise × vertical) instantaneous velocity maps with a PIV system, whose intrusiveness is limited to the introduction of solid targets for flow visualization. The PIV system consisted of an 8-bit 1600×1200 px² CCD camera and a double-cavity Nd-YAG laser with pulse energy of 30 mJ. PIV image pairs were acquired at a frequency of 15 Hz with a time delay of 1500 μs between frames. The solid targets used were polyurethane particles with density of 1.31 g/cm³. The size of the particles varied in between 50 μm and 70 μm and with a mean diameter of 60 μm (*c.f.* Ricardo, 2013, for details about the solid targets). For each plane acquired in test A, 10×573 px² images couples were collected, representing a total acquisition time of 6'37''. For test B, one dataset with 5000 image pairs was acquired at each vertical plane, corresponding to 5'33'' of consecutive data. Image pairs were processed with an adaptive correlation algorithm starting with interrogation areas of 128×128 px² and ending at 16×16 px², without overlap. The spatial resolution of the velocity maps yields to interrogation volumes of (0.7-1)×(0.7-1)×2 mm³, since the laser light sheet is approximately 2 mm thick.

Table 1 summarizes the main features of the experimental measurements for each measuring gap (M.Gap), where x is the longitudinal coordinate of the measuring gap relative to the flume's inlet, m is the stem areal number-density, $\mathrm{d}m/\mathrm{d}x$ is the longitudinal variation of m, U stands for the depth averaged of the double-averaged longitudinal velocity, H is the depth of the water column where the flow is controlled by the stems, $\mathrm{d}h/\mathrm{d}x$ is the gradient of the mean flow depth, h, and $Re_p = Ud/\nu$ is the stem Reynolds number, d being the stem diameter.

The experiments were run with a discharge of 2.3 l/s. The flow is gradually varied, accelerating in the downstream direction. The free surface exhibited an oscillating behavior with larger amplitude for dense patches.

Table 1. Features of the experimental measurements and flow properties for each measuring gap.

Test	M. Gap	x (m)	m (stems/m²)	$\mathrm{d}m/\mathrm{d}x$ (-)	U (m/s)	h (m)	$\mathrm{d}h/\mathrm{d}x$ (-)	H (m)	Re_p (-)
A	P1	6.680	1600	0	0.085	0.065	-0.020	0.046	1121
	P2	6.782	980	<0	0.083	0.064	-0.017	0.045	1158
	P3	6.935	400	0	0.090	0.063	-0.002	0.040	1237
	P4	7.036	980	>0	0.099	0.062	-0.012	0.045	1303
	P5	7.192	1600	0	0.103	0.057	-0.031	0.038	1302
	P6	7.293	980	<0	0.108	0.056	-0.018	0.036	1374
	P7	7.446	400	0	0.100	0.054	-0.010	0.036	1216
	P8	7.545	980	>0	0.106	0.052	-0.017	0.032	1222
B	Up	6.900	980	0	0.092	0.065	-	0.042	989
	Down	7.900	980	0	0.099	0.051	-0.014	0.041	1064

3. Results

3.1 Quantification of the time and space-averaged variables

This subsection presents the double-averaged velocity and stress profiles, which corresponds to the data used on the drag force computation. The length scale used to normalize the vertical coordinate of the profiles presented below corresponds to the depth of the water column where the flow is controlled by the stems, H. This region is identified by means of the inflection points in longitudinal form-induced stress profiles (details in Ricardo, 2013).

Figure 3 presents profiles of longitudinal and vertical velocities. For the longitudinal velocity, one can observe that the shape of the profiles is similar for all the tested m. There is a pronounced bulge, at lower layers, in almost all profiles, corresponding to a maximum of the mean longitudinal velocity.

The main feature of the longitudinal velocity within arrays of rigid stems is its uniform distribution on the region where the flow is controlled by the vertical elements. Profiles of vertical velocity show typically small values, except close to the bottom where, due to the interaction with the bed, the flow shows down- and upward movements (nevertheless presenting values one order of magnitude smaller than the longitudinal velocity).

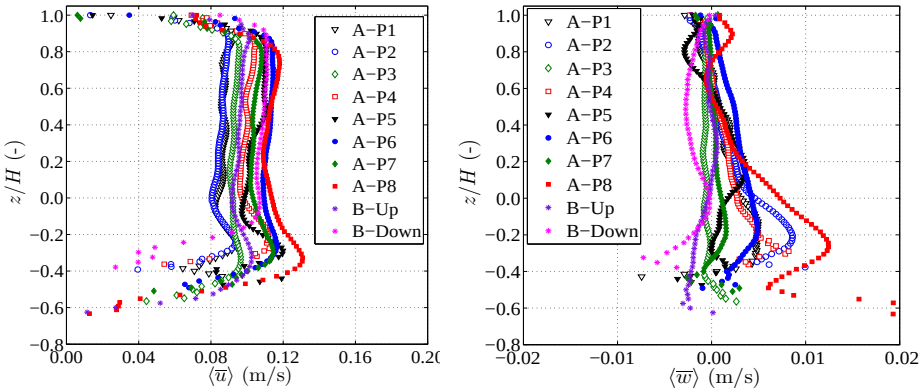

Figure 3. Vertical distribution of double-averaged longitudinal velocity (left) and vertical velocity (right).

Figure 4 represents Reynolds and form-induced shear stresses. The turbulent stresses have very small magnitudes, almost vanishing on the region controlled by the stems. Close to the bed and the free surface, patches with high stem areal number-density exhibit larger values. The form-induced shear stresses have the maximum values near the bottom and become almost zero reaching the free surface. These stresses are, in general, larger than Reynolds stresses and increase with the stem areal number-density.

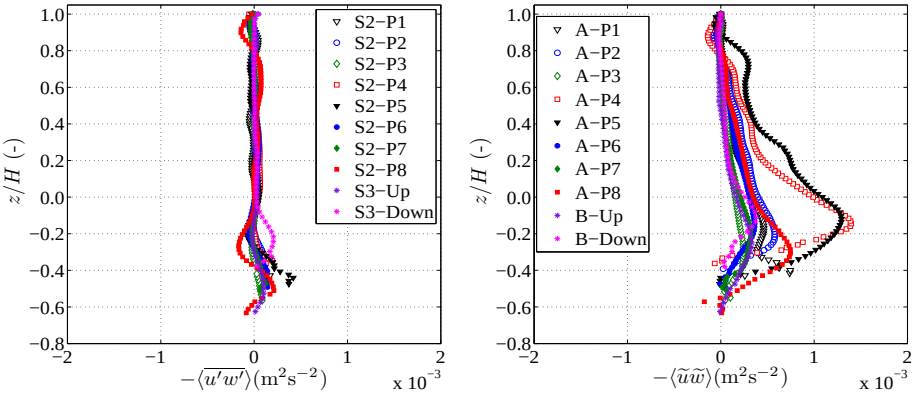

Figure 4. Vertical distribution of double-averaged Reynolds shear stresses (left) and form-induced shear stresses (right).

Normal longitudinal turbulent and dispersive stresses are presented in Figure 5, showing that both have the same order of magnitude and increase with the increasing m.

Vertical component of the Reynolds and form-induced stresses are shown in Figure 6. Reynolds normal vertical stresses exhibit an almost constant profile at most of the flow depth, decreasing to zero close to the bed and free-surface. Concerning the form-induced stresses, the magnitude is smaller than the corresponding turbulent stresses and the maximum values are found close to the bed, decreasing then to zero towards the free-surface.

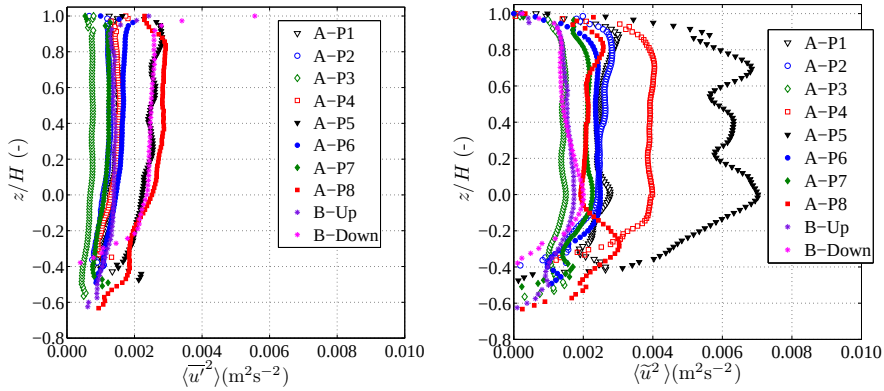

Figure 5. Vertical distribution of double-averaged Reynolds normal longitudinal stresses (left) and form-induced normal longitudinal stresses (right).

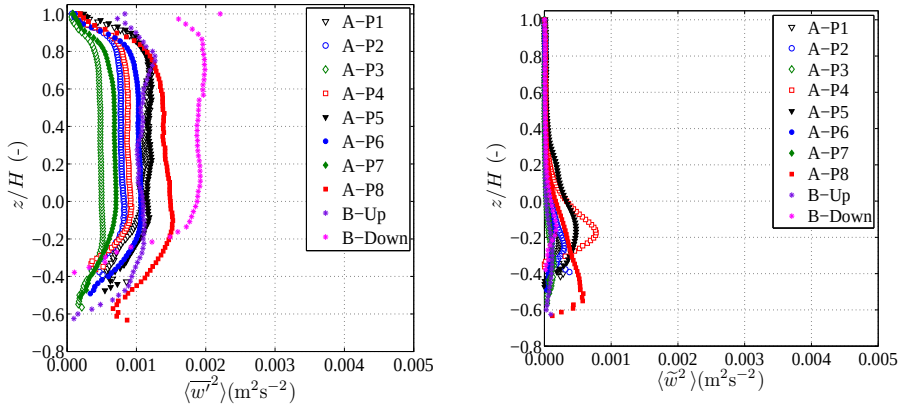

Figure 6. Vertical distribution of double-averaged Reynolds normal vertical stresses (left) and form-induced normal vertical stresses (right).

3.2 Quantification of drag forces

Integrating vertically the longitudinal component of Eq. [1], one obtains a conceptual formulation for computing the drag force acting on the stems.

Some simplifications were considered: measurements of horizontal velocity maps showed that $\langle \bar{v} \rangle \approx 0$; figures in the previous section showed that both turbulent and dispersive shear stresses vanish at the bottom and at the free-surface; the pressure distribution was considered hydrostatic; due to the high Reynolds number, the viscous stresses were assumed negligible; drag forces acting on the bottom are very small compared with those acting on the stems (Ferreira et al, 2009); it is assumed that the effect of $\phi^{(b)}$ is negligible, therefore it was considered $\psi = \phi^{(s)}$, which is constant through the flow depth since the stems are vertical. With this simplifications and incorporating the free-surface kinematic boundary condition, the mean drag force acting on the stems per unit of plan area, $\langle f_x^{(s)} \rangle$, is given by (*c.f.* Ferreira et al 2009 for details):

$$\langle\overline{f_x^{(s)}}\rangle = \frac{\rho}{\psi}\left(-\frac{\partial[\psi\langle\bar{u}\rangle\langle\bar{u}\rangle]}{\partial x}+\left[\langle\bar{u}\rangle\langle\bar{u}\rangle\frac{\partial\psi}{\partial x}\right]-g\frac{h^2}{2}\frac{\partial\psi}{\partial x}-g\psi\frac{\partial h}{\partial x}-\frac{\partial[\psi\langle\overline{u'u'}\rangle]}{\partial x}+\frac{\partial h}{\partial x}(\psi\langle\overline{u'u'}\rangle)|_h\right.$$
$$\left.-\frac{\partial[\psi\langle\tilde{u}\tilde{u}\rangle]}{\partial x}+\frac{\partial h}{\partial x}(\psi\langle\tilde{u}\tilde{u}\rangle)|_h\right) \quad [2]$$

where the brackets represent integral variables as $[\theta\,] = \int_0^h \theta \mathrm{d}z$.

The mean drag force per unit of submerged stem length is defined as $F_D = \langle\overline{f_x^{(s)}}\rangle/mh$. The mean drag force in the longitudinal direction is often defined in literature as the force that balances the pressure gradient (Tanino and Nepf, 2008) by $F_D^* = -\psi\frac{\rho g}{m}\frac{\mathrm{d}h}{\mathrm{d}x}$. Figure 7 shows the values of F_D and the simplification F_D^* against m. Although the pressure gradient is the dominant term in the drag force, Figure 7 indicates that balancing the drag force only with this term may lead to important non-systematic errors.

A clear correlation between F_D and m was not found. It seems that F_D decreases with m but only for the highest values of F_D. If the mean of all points for each m is considered, F_D appears approximately constant. To discuss the impact of the variability of m on F_D, the results at m=980 stems/m² should be analyzed. In test A, patches $p_{1\text{-}2}$ and $p_{2\text{-}6}$, which present decreasing m, exhibit larger values of drag force than patches $p_{3\text{-}4}$ and $p_{7\text{-}8}$, where m increases longitudinally. While test B, with constant m, is characterized by an intermediate value of F_D.

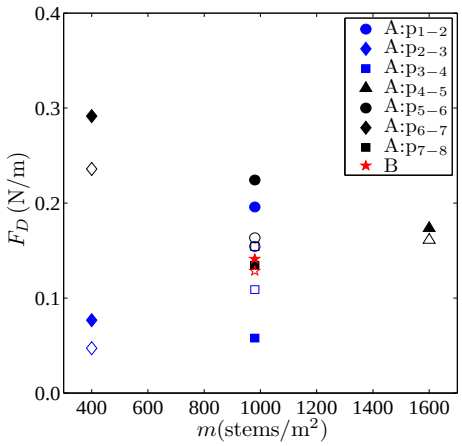

Figure 7. Drag force per unit of length of submerged stem, F_D, as function of the stem areal number-density, m. The filled markers represent the drag force computed based in Eq. [2] while the open markers corresponds to the simplification F_D^*.

3.3 Drag coefficient

The drag coefficient, defined as $C_D = 2F_D/(\rho d U^2)$, is presented in Figures 8 and 9 as function of the stem Reynolds number, flow depth gradient, flow depth and the mean inter-stem space $(s = 1/\sqrt{m})$. The latter two parameters were considered normalized by the stem diameter, d.

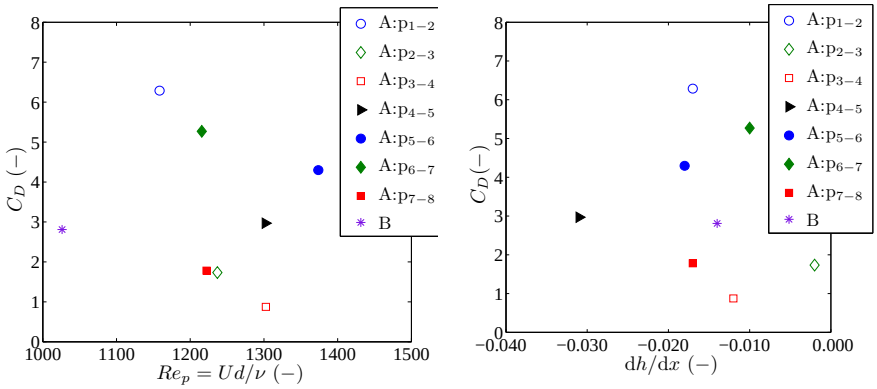

Figure 8. Dependence of the drag coefficient, C_D, on the stem Reynolds number Re_p (left) and on the gradient of the flow depth dh/dx (right).

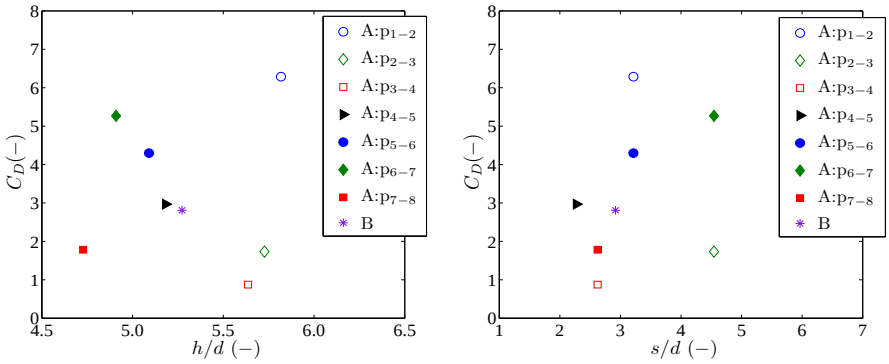

Figure 9. Dependence of the drag coefficient, C_D, on h/d (left) and on s/d (right).

The correlation between C_D and Re_p, presented in Figure 8, does not reveal a clear tendency. Due to the small magnitude of viscosity, viscous forces are expected to be negligible, then C_D is not expected to vary with Re_p. The unsystematic distribution of values obtained in the present work may express the influence of other parameters on C_D or experimental errors.

The flow depth gradient,dh/dx, is proportional to the dominant term of the drag force, then the increase of C_D with the magnitude of the flow depth gradient was expected. Worth to note is the sorting of the transition reaches on test A and test B, in terms of local m. These reaches have very similar mean stem areal number-density, however due to the random stem distribution, locally the flow may find regions with higher or lower density of stems.

The parameter h/d expresses the influence of the bed on the definition of the flow structure, being higher values of h/d associated with a smaller relative influence of the bed. Figure 9 shows a tendency for the decrease of C_D with increasing h/d, what means that the contributions of the boundary-layer flow near the bottom, subjected to velocities lower than the depth-averaged mean velocity, contributes more than the average, along the water column, to the drag force. Exceptions for this trend are the patches $p_{1\text{-}2}$ and $p_{7\text{-}8}$, which are transition patches.

A positive correlation between C_D and s/d is shown in Figure 9, indicating a decrease of C_D with increasing m. Most of published works claim an increase of C_D with m; however it must be underlined that conditions may vary considerably from one study to another, namely the form of calculating F_D, not allowing a direct comparison.

4. Conclusions

This work was aimed at the quantification of the drag forces, and respective coefficients, for flows within boundaries covered by rigid and emergent vegetation, with varying and constant stem areal number-density. It allowed for the following main conclusions:

- the form-induced stresses should not be neglected as they are of the order of magnitude of Reynolds stresses;
- the simplification of balancing the drag force only with the pressure gradient may lead to important errors;
- F_D seems uncorrelated with m, but the former depends on the longitudinal variation of the latter;
- C_D does not vary with Re_p, for the investigated range of Re_p and m;
- decrease of C_D with increasing h/d reveals an influence of the bed on the definition of the flow structure;

Acknowledgments

This study was funded by the Portuguese Foundation for Science and Technology through the project PTDC/ECM/117660/2010.

References

Aberle, J. and Järvelä, J. (2013). 'Flow resistance of emergent rigid and flexible floodplain vegetation.' *Journal of Hydraulic Research*, 51(1), 33–45.

Ferreira, R. M. L., Ricardo, A. M., and Franca, M. J. (2009). 'Discussion of 'Laboratory investigation of mean drag in a random array of rigid, emergent cylinders' by Heydi M. Nepf and Yukie Tanino, Journal of Hydraulic Engineering, vol. 134, no 1, 2008.' *Journal of Hydraulic Engineering*, 135(8), 690–693.

Finnigan, J. (2000). 'Turbulence in plant canopies.' *Annu. Rev. Fluid Mech.*, 32, 519–571.

Franca, M. J. & Czernuszenko, W. (2006). 'Equivalent velocity profile for turbulent flows over gravel riverbeds.' In: *River Flow 2006* (R. M. L. Ferreira, J. G. A. B. L., E. C. L. Alves & Cardoso, A. H., Eds.). Taylor and Francis.

Kadlec, R. H. (1990). 'Overland flow in wetlands: Vegetation resistance.' *Journal of Hydraulic Engineering*, 116(5), 691–705.

Nikora, V., Mcewan, I., Mclean, S., Coleman, S., Pokrajac, D. and Walters, R. (2007). 'Double-averaging concepts for rough-bed open-channel and overland flows: Theoretical background.' *Journal of Hydraulic Engineering*, 133(8), 873–883

Ricardo, A.M. (2013). Hydrodynamics of Turbulent Flows Arrays Of Circular Cylinders. PhD thesis, EPFLausanne and IST-ULisboa.

Tanino, Y. and Nepf, H. M. (2008). 'Laboratory investigation of mean drag in a random array of rigid, emergent cylinders.' *Journal of Hydraulic Engineering*, 134(1), 34–41.